GENERAL ELECTRIC REVIEW

Published by
General Electric Company's Publicity Department
Schenectady, New York

Stress Distribution in Electric Railway Motor Pinions as Determined by the Photo-elastic Method

By PAUL HEYMANS and A. L. KIMBALL, Jr.

REPRINT

From Issue of March, 1923

July, 1925

GEA-95
Old Series X-703-3

Stress Distribution in Electric Railway Motor Pinions as Determined by the Photo-elastic Method

By PAUL HEYMANS, Cambridge, Mass.
and A. L. KIMBALL, JR., Research Laboratory, General Electric Company

This article embodies some results of a general scientific study undertaken for the development of superior electric-railway motor pinons. The particular portion of the work described was performed at the Massachusetts Institute of Technology, using the General Electric Company's apparatus for stress determination in transparent models by the photo-elastic method. Some of the supplementary mechanical tests were made at Schenectady, and throughout the work close contact was maintained with the Railway Motor Department and the Research Laboratory at Schenectady. A brief description and discussion of the photo-elastic method is given in the first part. The stress distribution in, and the causes of ruptures of, given types of gear pinions used in electric-railway motors, as investigated by the photo-elastic method, are afterward reported upon and discussed. This article was presented as a paper at the annual meeting, New York, December 4 to 7, 1922, of the American Society of Mechanical Engineers.—EDITOR.

I. DESCRIPTION OF THE METHOD

How to Define the State of Stress at any Point of a Solid Body

The state of stress at any point in a solid body is determined when the traction across every plane through the point is known. There exist at any point three orthogonal planes across which the traction is purely normal and which are called the planes of principal stress. The normal tractions across those planes are called the principal stresses. The state of stress at any point is completely determined by the direction and the magnitude of the principal stresses at the point under consideration. The principal stresses, given in direction and in magnitude, express in the most general and complete way the elastic state at any given point. The bending moment, the shearing forces, etc., are readily deduced from the direction and the magnitude of the principal stresses. Furthermore, one of the principal stresses always expresses the maximum stress.

2. The notion of principal stress may be illustrated as follows:

3. Consider a spherical element in a solid body. External applied loads will deform this spherical element into an ellipsoidal element (Fig. 1). The axes of this ellipsoid will correspond in direction and in magnitude to the direction and the magnitude of the principal stresses.

4. The orientation and the form of the ellipsoid, and therefore the direction and the magnitude of the principal stresses, will define the state of stress at the point under consideration.

5. The axes of the ellipsoid represent the largest and the smallest deformation at the point under examination. Correspondingly, the principal stresses give the direction and the magnitude of the maximum and the minimum stress.

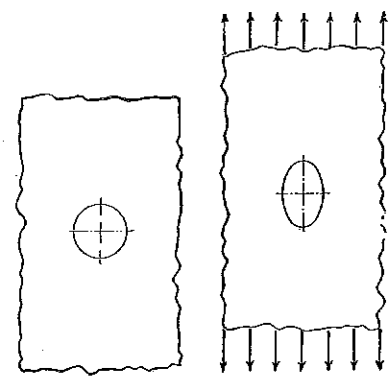

Fig. 1. Ellipsoidal Element Resulting from Subjecting a Spherical Element to Stress

6. If the three principal stresses vary from point to point in the structure, the problem to be dealt with is a three-dimensional elastic one. If one of the three principal stresses vanishes throughout, it is a two-dimensional elastic or plane-stress problem.

7. Corresponding to the three- and two-dimensional elastic-stress problems there are also the three- and two-dimensional elastic-strain problems, when the deformations corresponding to the principal stresses are considered.(1)

8. A great number of structural problems (bridge, ship, airplane, plate, dam, etc., construction) are, or their stress analysis may be reduced to, two-dimensional elastic problems.

(1) A complete theory of stress and strain may be found in the "Treatise on the Mathematica Theory of Elasticity," by A. E. H. Love, 3d ed., chapters i-iv.

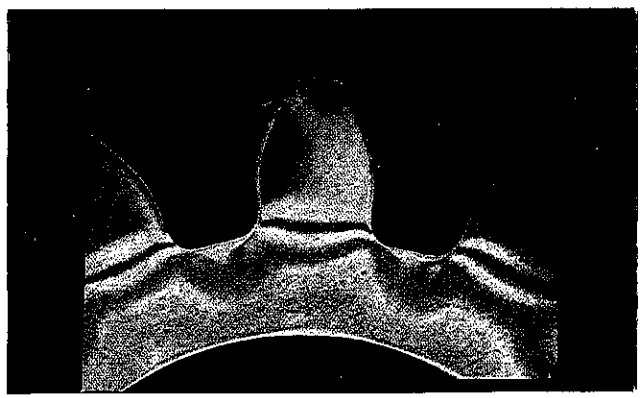

FIG. 2. COLORED IMAGE WHEN NORMAL INSIDE PRESSURE ALONE IS APPLIED

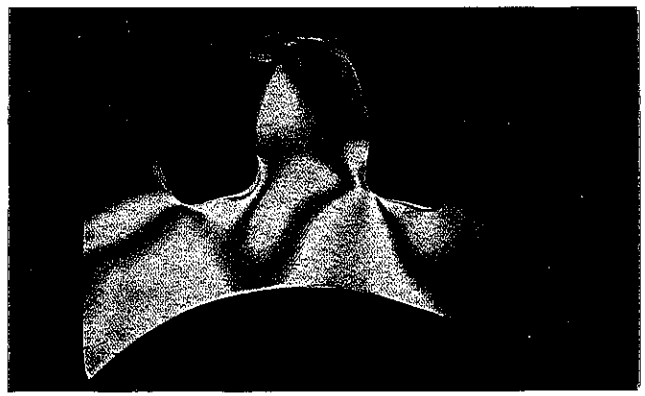

FIG. 5. COLORED IMAGE OBTAINED FOR NORMAL INSIDE PRESSURE AND REDUCED TORQUE

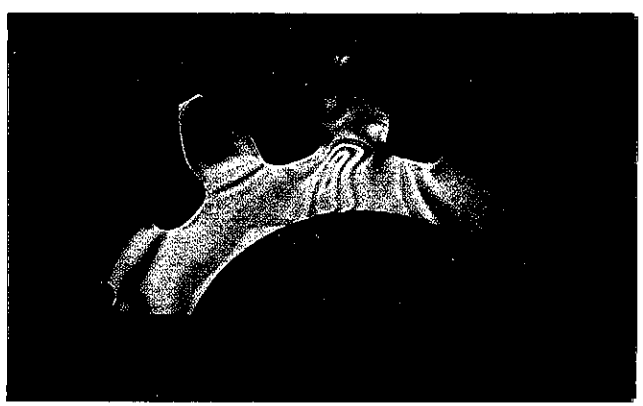

FIG. 3. COLORED IMAGE WHEN BOTH NORMAL INSIDE PRESSURE AND MAXIMUM TORQUE ARE APPLIED

FIG. 4. COLORED IMAGE WHEN BOTH NORMAL INSIDE PRESSURE AND MAXIMUM TORQUE ARE APPLIED

The Photo-elastic Method of Stress Determination

9. As set forth in Par. 1, the state of stress at any point is most completely defined by the direction and the magnitude of the principal stresses. These are, therefore, the elements which we wish to determine for a complete analysis.

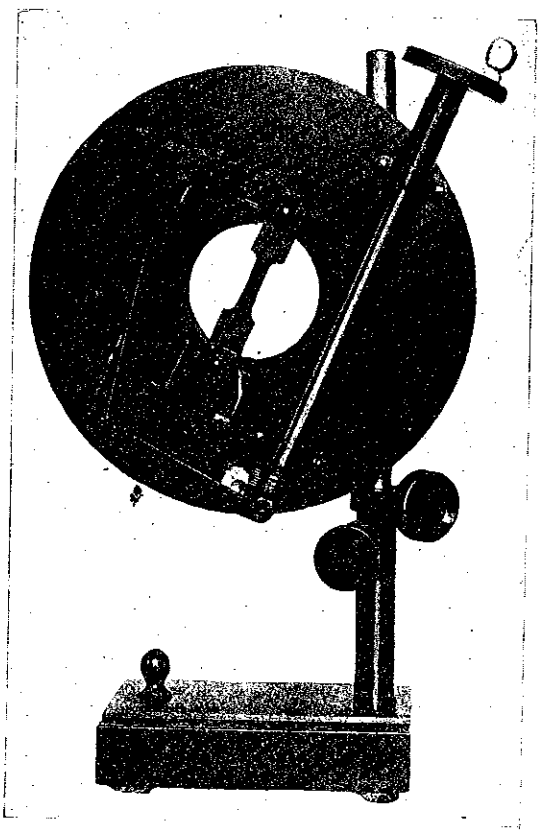

Fig. 6. Frame for Comparison Member Designed by E. G. Coker and A. L. Kimball, Jr.

10. The photo-elastic method solves the two-dimensional elastic problems. It primarily takes advantage of the double refracting properties shown by isotropic transparent substances when put under stress. The stresses in the structure may therefore be determined from models made of a homogeneous transparent material, and ordinarily on a reduced scale. The stresses in a steel, cement, or any other structure, homogeneous throughout and obeying Hooke's law of linear proportionality between stress and strain, may be readily deduced from the values obtained by the analysis of the corresponding transparent model for the case of two-dimensional elastic problems.

11. If plane polarized light is passed through a stressed specimen of celluloid and afterward through a second nicol prism whose principal section is parallel to the plane of polarization of the original beam of light, only the points where the principal stresses are respectively parallel and perpendicular to the principal sections of the crossed nicols remain dark. This result makes it possible to determine the directions of the principal stresses at any given point. Moreover, this information is needed for the measurements which will be described later.

12. If now circularly polarized light be passed through the specimen, by interference of the two component rays, which in the double-refracting specimen have suffered a relative retardation at each point proportional to the difference in magnitude of the two principal stresses, a colored image is obtained. (Figs. 2, 3, 4 and 5.)*

13. By a comparison method, based upon the interposition in the proper direction of a comparison member of constant cross-section, put under uniform tension in a suitable frame (Fig. 6), the value of the difference of the principal stresses at any given point may be read on the dynamometer of the frame.

14. Now, in the two-dimensional elastic problems the transverse deformation, i.e., the deformation along a normal to the plane of the two principal stresses, is proportional to the sum of those two stresses. By means of a lateral extensometer (Fig. 7), we measure this transverse deformation.

15. From the values of the differences and the sums of the principal stresses, the separate values of each of them are computed, thus determining completely the state of stress.

16. A question naturally arising is whether the results obtained on a transparent body such as celluloid hold for structural materials.

17. It is shown by the general discussion of the equations of elastic equilibrium that in the case of strain or plane stress in an isotropic body obeying Hooke's law of linear proportionality between stress and strain, the stress distribution is independent of the moduli of elasticity and consequently of the material of which the body is made. Thus the stress distribution experimentally determined in the case of a celluloid body is the same as it is when the body is made of any other isotropic substances such as iron, steel, etc., obeying Hooke's law, in distribution,

*See Frontispiece of this issue of the REVIEW.

direction, and magnitude.[1] Moreover these conclusions derived from the general theory of elasticity have been checked by experiment.[2]

18. The photo-elastic method can be applied to the great majority of structural problems, not only in taking the place of mathematical computation, but particularly in solving those structural problems where mathematics become too involved to be of help. Moreover it has the great advantage of giving the maximum stress at each point throughout the whole structure, and it therefore offers an effective means of increasing safety and reducing superfluous material.

II. A STUDY OF THE STRESS DISTRIBUTION IN GEAR PINIONS

19. When accidents occur with gear wheels, besides the metallurgical question, three possible causes of failure suggest themselves:

a. The gear wheel may not have been properly designed.

b. It may have failed under an excessive load.

c. When the pinion was shrunk hot or forced on to a tapered shaft, an excessive inside radial pressure may have been set up.

20. It is easy to see that the ordinary methods of resistance calculations of gear wheels, based on considering the tooth as a cantilever loaded at its end, would not be expected to give reliable and complete information as to stress distribution, not even for the root section of the tooth which is under consideration.

21. Indeed, the shape of the tooth, the curvature at the root, the ratio of the diameter of the pinion bore to the root and outside diameter, the permanent stresses introduced by the placing of the pinion on the shaft, etc., all affect the stress distribution and the maximum stress. Photo-elastic analysis shows that these factors affect the stresses considerably more than would be expected from present methods of estimating. For standardized pinions the correction coefficients can only partially take account of these factors. For special pinions or for pinions of which more efficient running is required, a photo-elastic analysis seems to be the best if not the only effective way to determine the stress distribution and to locate the maximum stress.

22. A detailed analysis of the stress distribution determined for different gear pinions

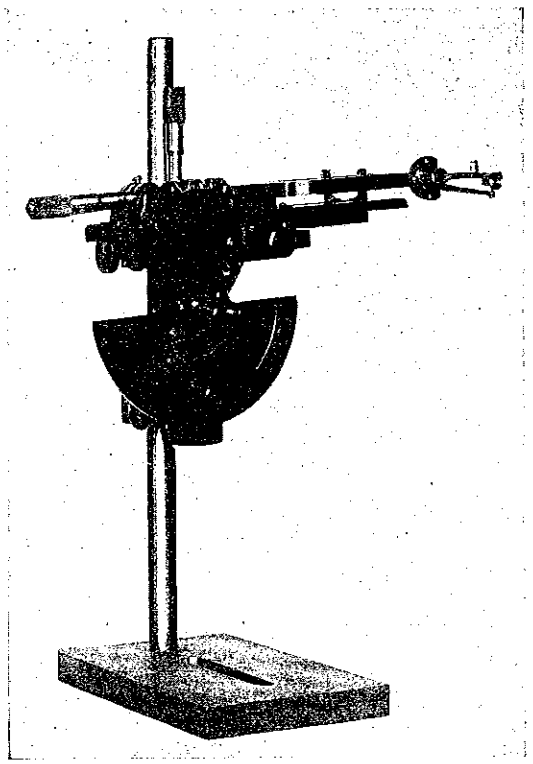

Fig. 7. Lateral Extensometer Designed by P. Heymans

and under different loading conditions is given below.

23. The authors wish first to call attention to certain interesting points brought out by photo-elastic analysis, which have been checked by tests carried out on steel sections. These are particularly interesting because they are unexpected.

24. Besides the stress distribution in the different sections of the pinions represented by Fig. 8, the photo-elastic analysis has given as maximum stress under normal inside radial pressure and normal torque:

80,000 lb. per sq. in. for tooth form *A*
70,350 lb. per sq. in. for tooth form *B*
60,900 lb. per sq. in. for tooth form *C*

Moreover the 12-tooth pinion shows, besides a smaller maximum stress, a better stress distribution.

---

(1) Except, however, if the body is multiple connected and the resultant applied forces do not vanish separately over each boundary. In this particular case the correction coefficients for passing from one isotropic substance to another may be experimentally determined. ("On Stresses in Multiple-connected Plates," by L. N. G. Filon, British Assn. Report, 1921.)

(2) "Photo-elastic Measurements of the Stress Distribution in Tension Members Used in the Testing of Materials," by E. G. Coker, Excerpt Proc. Inst. C. E. (London),—vol, ccvii, part II, p. 8.

"Photo-elastic and Strain Measurements of the Effects of Circular Holes on the Distribution of Stress in Tension Members," by E. G. Coker, Trans. Inst. Engrs. & Shipbuilders in Scotland, vol. lxiii, part I, p. 33.

"La Photo-elasticimétrie, ses principes, ses méthodes et ses applications," by Paul Heymans. Bull. Soc. Belge Ing. et Ind., Aug., 1921, pp. 147-154, 165-167, 189-199.

25. For steel pinions the maximum stress attained under normal conditions, although high, appears not to be excessive. *Tooth C appeared to be a better design* under normal conditions.

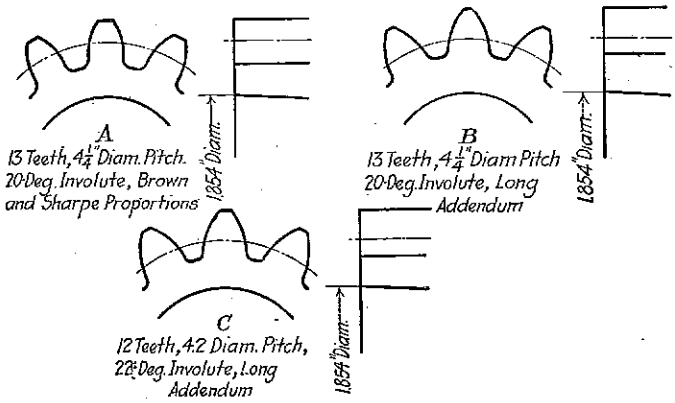

Fig. 8. Tooth Forms of Pinions Subjected to Photo-elastic Analysis

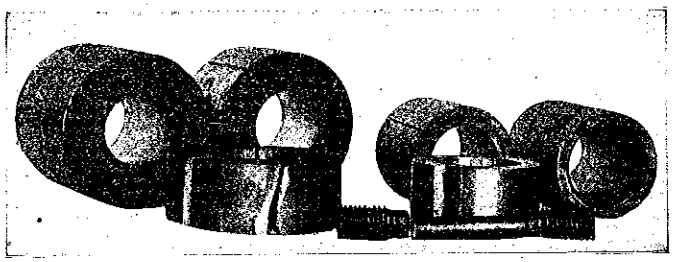

Fig. 9. Steel Rings Ruptured by Being Forced onto a Tapered Plug

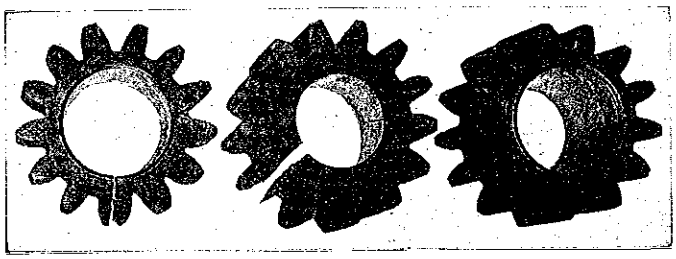

Fig. 10. Steel Pinions Ruptured by Being Forced onto a Tapered Plug

26. The stresses due to shrinking or forcing the pinion on the shaft can only be estimated. The pinion may be assumed to be a plain circular ring for which case the stresses may be mathematically computed. The stress at any point of the ring as well as the maximum stress in the ring depends upon the lengths of the inside and outside radii. The opinion generally expressed is that for the case of the pinion the maximum stress will be intermediate between the maximum values obtained for rings of which the outside diameters are respectively equal to the root diameter of the tooth and to the outside diameter of the pinion, the inside bore being the same.

27. Photo-elastic analysis shows that *the gear pinion is even weaker than the plain circular ring whose outside diameter is equal to the root diameter of the tooth.* The change of external profile, due to the presence of the teeth, although requiring an addition of material, weakens the structure.

28. Figs. 9 and 10 show the steel specimens after having been tested by forcing a tapered plug into the bore; and Table I gives the rupture load applied to the tapered arbor forced into the bore for the different specimens. These confirm the photo-elastic results.

29. Previous to the photo-elastic investigation of the stresses due to radial inside pressure in pinion sections, fracture due to pure radial inside pressure would have been expected to occur through the minimum radial cross-section.

30. From Fig. 2,* representing the color image obtained in the photo-elastic analysis, it appears that *the regions under the teeth are under higher stress* and that the points at the inside boundary right under the teeth are points of maximum stress.

31. Fig. 10 gives the fracture obtained on steel sections. Two of the sections show fractures right through the thickest layer of material, while all of them started at points where the photo-elastic analysis had revealed maximum stress. The unevenness of the material must account for the deviation of the fracture in one of the cases.

32. Can any statement be made as to the causes of the failure by inspection of the shape of the fracture? In the case in which the authors were interested, the photo-elastic analysis determined the best design. As before said, either the placing of the pinion on the shaft, if carelessly done, for instance by pounding the pinion heavily on the tapered

*See Frontispiece of this issue of the REVIEW.

shaft, or excessive torque and blows due to sudden meshing or the taking on of a heavy load, will set up dangerous stresses.

TABLE I
RUPTURE LOAD ON AREOR FORCED INTO SPECIMENS TESTED

	Inside Diam., In.	Outside Diam., In.	Root Diam., In.	Rupture Load, Lb.
Ring.....	1.854	3.5	....	85,000
Ring.....	1.854	2.5	....	51,000
Pinion.....	1.854	3.5	2.5	47,000

33. The author's photo-elastic analysis has shown that *the sections of dangerous stresses*

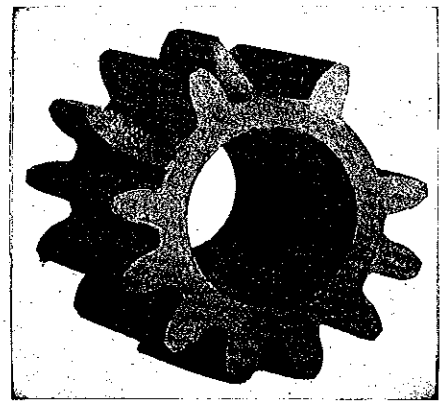

Fig. 11. Fatigue Failures of Teeth Produced by Experiment (without Radial Pressure in Bore)

are different for different values of inside radial pressure and applied torque load.

34. The fracture shown in Fig. 11 is of an *open* V-shape. Photo-elastic analysis shows that *the higher the inside radial pressure becomes*, for a given torque load, *the sharper becomes the V-shape of the section of dangerous stresses.* (Fig. 12.) If the fracture is due to too high a torque load, the angle of the V will approach 180 deg. Tests on steel sections have been made with a specially built impact machine.

35. Without inside radial pressure the fracture obtained is a straight line through the root section of the tooth. With increasing pressures the V-shaped fracture becomes sharper. For an inside radial pressure exceeding the elastic limit, however, the observation does not hold. The reason for this departure from what the photo-elastic method had predicted is to be found in the fact that beyond the elastic limit the stress-and-strain relation no longer follows Hooke's law. Therefore the stresses set up in the steel pinions by the shrinking process no longer correspond with those set up in the celluloid model.

36. While the flat shape of the break in Fig. 11 is one limiting case (torque without radial shrinking pressure), Fig. 10 may be considered as the other limiting case (radial shrinking pressure without torque), showing a V-shaped fracture for which the angle of the V has become equal to zero.

37. It may be concluded, then, that the inspection of the fracture may be a means of determining the cause of the failure. In this way, possibly, the responsibility may be established between builder and customer as regards pinion mounting.

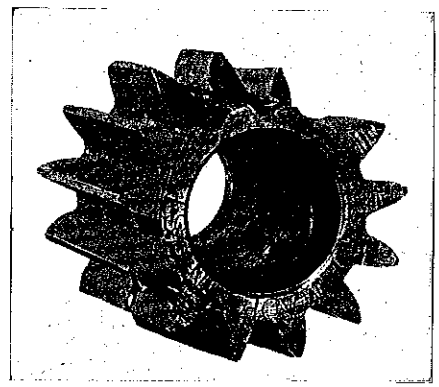

Fig. 12. Fatigue Failures of Teeth Produced by Experiment (with Heavy Radial Pressure in Bore)

The Detailed Stress Analysis

38. *External Forces Applied to the Pinion When in Service.* The pinion is shrunk onto the shaft after having been bored so as to fit the shaft at a temperature of 160 deg. F. above normal room temperature.

39. In normal working conditions, the torque load to which the pinion is subjected corresponds to a tractive force of 500 lb. per inch of face of the tooth, tangent in direction to the pitch circle. The whole torque is supposed to be transmitted by a single contact.

40. Calling respectively $\widehat{rr}$ and $\widehat{\theta\theta}$ the radial and the tangential principal stress in a circular ring, of which the outside diameter equals the root diameter of the teeth, the inside bore being the same as the pinion bore, $(\widehat{rr}-\widehat{\theta\theta})$ = 28,800 lb. per sq. in. for $\triangle t = 160$ deg. F. This value of $(rr-\widehat{\theta\theta})$ is the stress value of the color bands obtained in polarized light (isochromatic bands), and will therefore be used

in the stress analysis of the celluloid model to secure the right expansion pressure before the torque is applied. For radial pressures higher than this normal shrinking pressure, the same characteristic of the $(\widehat{rr}-\widehat{\theta\theta})$ value will be used.

41. The tangential tractive force is applied at varying distances from the root of the tooth, depending upon the point of contact. The most unfavorable conditions arise when this force is applied at the top of a single tooth. Moreover, the starting torque load being higher than that realized under normal running conditions, the applied tractive force was brought up from 500 lb. to 1500 lb. per inch of face.

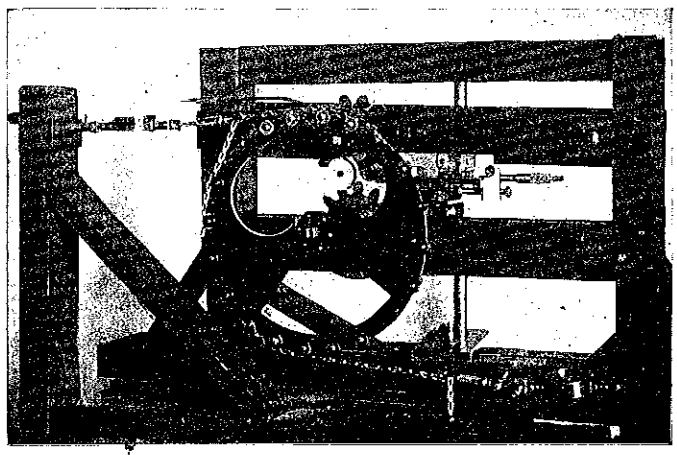

Fig. 13. Frame Used for Applying Loads to Celluloid Models of Pinions

42. Let us for convenience call:

a. The *normal* inside pressure, the value of 28,800 lb. per sq. in. for $(\widehat{rr}-\widehat{\theta\theta})$, corresponding to a shrinking pressure due to a temperature variation of 160 deg. F.

b. The *maximum* torque, the torque corresponding to a tractive load F of 1500 lb. applied normally to the contour of the tooth (condition of contact) at the top of one pinion tooth.

c. The *normal* torque, the torque corresponding to a tractive load F of 500 lb. applied under the same conditions as above.

d. *Increased* inside pressures, the values of $(rr-\widehat{\theta\theta})$ exceeding the normal inside pressure, as defined above.

43. *The Photo-Elastic Analysis.* Fig. 13 represents the frame used for the loading of the models. A tapered expansion ring is used to produce the radial inside pressure. The torque is measured by properly mounted dynamometers.

*See Frontispiece of this issue of the REVIEW.

44. The first sets of measurements were made under normal inside pressure and maximum torque load. Fig. 14 represents the lines of principal stress, deduced from the isoclinic bands. The tangents to these lines represent at each point the directions of the principal stresses.

45. Fig. 2* gives the colored image when the normal inside pressure alone is applied, whereas Figs. 3* and 4* give the image obtained when both the normal inside pressure and the maximum torque are applied. An optical measurement on the image shown in Fig. 2* allows one to adjust properly the amount of inside pressure before the torque is applied.

46. The determination of the values of the difference $(p-q)$ of the principal stresses is made on the image shown in Fig. 4.* One of the two principal stresses vanishes at a boundary where no external forces are applied. In this case the optical measurements of the values of $(p-q)$ give directly the values of the tangential stress.

47. Inside of the body the optical measurements are supplemented by measuring the transverse change of thickness, which gives the values of the sum $(p+q)$ of the principal stresses.

TABLE II

VALUES OF THE PRINCIPAL STRESSES ACROSS THE MINIMUM CROSS-SECTION OF THE LOADED TOOTH

Tenths of Distance AB (Fig. 15) Measured from A	p Lb. per Sq. In.	q Lb. per Sq. In.
0	0	72,600
0.1	13,850	57,300
0.2	10,450	49,000
0.3	3,710	41,700
0.4	−10,620	25,800
0.5	−20,300	18,700
0.6	−29,000	11,900
0.7	−40,000	9,000
0.8	−51,900	.....
0.9	−65,700	5,320
B	−80,000	0

48. From the values of the principal stresses at a given point it is easy to obtain the stress on a section in any given direction at that point. Moreover, as said before, the two principal stresses represent respectively the maximum and the minimum stress. Thus the larger of the principal stresses will always

give at each point the maximum stress in direction and magnitude.

49. At the edges where one of the principal stresses has vanished the values of $(p-q)$ and $(p+q)$ must correspond, i.e., the optical determination of $(p-q)$ and the determination of $(p+q)$ must check.

50. Also, if we know the total force acting normally to a given section, the graphical integral of the curve, obtained by plotting the resultant stresses acting normally to this section, must correspond to the total force. In the case of the pinions the data for such a check are not available.

51. Table II gives the values of the principal stresses through the minimum cross-section of the pinion tooth, to which the load is applied. The results given in this table have been plotted in Fig. 15. At each point where measurements have been made the two principal stresses have been plotted in direction and in magnitude, the arrows serving to distinguish between tension and compression. At the points A and B $(p-q)$ and $(p+q)$ must check: they differ for A by 0.9 per cent and for B by 0.8 per cent.

52. The maximum tension occurs at A and is equal to 72,600 lb. per in. The maximum compression occurs at B and is equal to 80,000 lb. per sq. in. This difference between the absolute values of these stresses is of course due to the pressure on the inside of the pinion, which affects the tension and the compression stresses differently.

53. Figs. 16 and 17 give the values of the tangential stresses along the edge of the tooth on which the load is applied. The numerical results of Table III have been plotted in Fig. 16, this table giving the tangential stresses at the tension side. Also the numerical results of

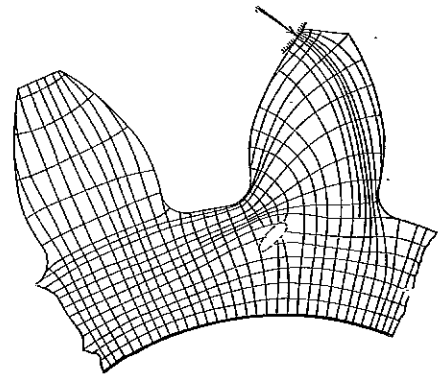

Fig. 14. Lines of Principal Stress Determined by Polarized Light—Normal Inside Pressure and Maximum Torque Load

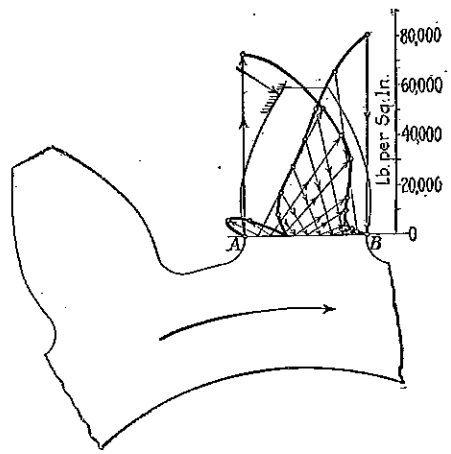

Fig. 15. Curves showing the Two Principal Stresses in Direction and Magnitude for Points Along the Section AB

TABLE III

VALUES OF THE TANGENTIAL STRESS AT THE BOUNDARY OF THE LOADED TOOTH—TENSION SIDE

No. of Point in Fig. 16	q Lb. per Sq. In.	
1	41,000	
2	54,100	
3 (A)	72,300	72,750[1]
4	73,200	
5	64,800	
6	57,600	
7	54,100	
8	41,000	
9	.....	

[1] Value obtained by taking $\frac{1}{2}[(p+q)+(p-q)]$, the other values being $(p-q)$ measurements.

TABLE IV

VALUES OF THE TANGENTIAL STRESS AT THE BOUNDARY OF THE LOADED TOOTH—COMPRESSION SIDE

No. of Point in Fig. 17	p Lb. per Sq. In.	
1	20,500	
2	41,000	
3 (B)	79,500	80,000[1]
4	80,000	
5	82,200	
6	60,000	
7	29,000	
8	0	

[1] Value obtained by taking $\frac{1}{2}[(p+q)+(p-q)]$, the other values being $(p-q)$ measurements.

Table IV have been plotted in Fig. 17, this table giving these stresses on the compression side. Since no external load is applied at this side, the optical measurements give the values of the tangential stresses up to the top of the tooth.

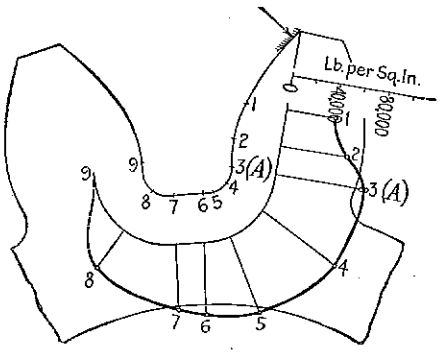

Fig. 16. Tangential Stress at Tension Side—Normal Inside Pressure and Maximum Troque

54. Table V and Fig. 18 give the numerical and plotted values of the stress difference $(rr-\widehat{\theta\theta})$ along the inside boundary of the pinion, the normal inside pressure and the torque load being applied. A circular ring to which a uniform inside pressure is applied will show concentric isochromatic bands. The deflections of those bands (Fig. 2)* in the case of the pinion show the disturbance due to the presence of the teeth.

55. When the maximum torque is applied, the values obtained for $(rr-\widehat{\theta\theta})$ give the curve of Fig. 18. The colored images as well as the diagrams show that the load applied at the top of one tooth extends its influence as far as the inside boundary of the pinion. The combination of the inside uniform pressure, already disturbed by an irregular outside boundary, with irregularly distributed stresses—tensions in certain parts and compressions in others—due to the torque load, do not of course give a resultant stress distribution which shows any symmetry with respect to the point of contact. The upper pinion being the driving pinion, it may be seen on the colored image (Fig. 3)* that the stresses vanish rather rapidly in the withdrawing part, but that the penetration extends much farther into the approaching part.

56. It may also be interesting to point out that there is a zone of zero stress inside of the pinion under the root of the tooth when the torque load is applied. This is shown on the diagram of the lines of principal stress (Fig. 14) by the converging of the lines of principal stress. Where several lines of principal stress intersect, the principal stresses usually vanish.

57. The question of engineering interest was to find the relative influence of the factors which affect the maximum stress, and the authors therefore varied the values of:

a. The inside normal pressure

b. The torque load.

TABLE V

VALUES OF $(\widehat{rr}-\widehat{\theta\theta})$ ALONG THE BOUNDARY OF THE BORE

No. of Point in Fig. 18	$(\widehat{rr}-\widehat{\theta\theta})$ Lb. per Sq. In.
1	36,600
2	54,100
3	36,600
4	18,100
5	41,000
6	61,500
7	43,500
8	38,700

58. The values of $(rr-\widehat{\theta\theta})$ along the inside boundary when the maximum torque load is applied are given in Table VI and have been plotted in Fig. 19 for the case of reduced inside pressure. The colored image did not show noticeable variation across the minimum cross-section AB and along the outside edges of the main tooth. The influence of the inside

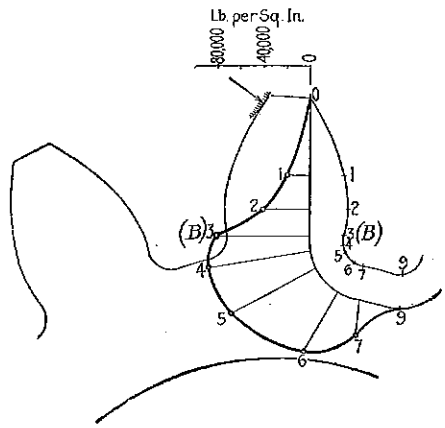

Fig. 17. Tangential Stress at Compression Side—Normal Inside Pressure and Maximum Torque

pressure on the above-mentioned limit does not affect materially the regions of maximum stress, due in this case to the torque load.

59. Fig. 5* shows the image obtained for normal pressure and reduced torque. Having applied 0.7 of the maximum torque value, the

*See Frontispiece of this issue of the REVIEW.

stresses showed a general reduction in the region of high stress. The values of the tangential stresses along the tension side of the boundary of the main tooth are given in Table VII and are plotted in Fig. 20. This should be compared with the same diagram (Fig. 16) for

TABLE VI

VALUES OF $(\widehat{rr}-\widehat{\theta\theta})$ ALONG THE BOUNDARY OF THE BORE

(Maximum torque—reduced radial pressure)

No. of Point in Fig. 19	$(\widehat{rr}-\widehat{\theta\theta})$ Lb. per Sq. In.
1	37,600
2	36,600
3	20,500
4	14,550
5	20,500
6	36,600
7	54,100
8	54,100
9	41,000
10	20,500

the case where the full load is applied. The maximum tension has dropped from 73,200 lb. per sq. in. (Table II) to 57,700 lb. per sq. in. (Table VII); i.e., it has been reduced to 0.8 of its previous value. The fact that it has dropped only to 0.8, whereas the torque was reduced to 0.7, is explained by the permanent stress due to the inside radial pressure which had been maintained at its previous value. A reduction of the torque load has as a result a reduction of the maximum stress. We shall see later that this is not always the case.

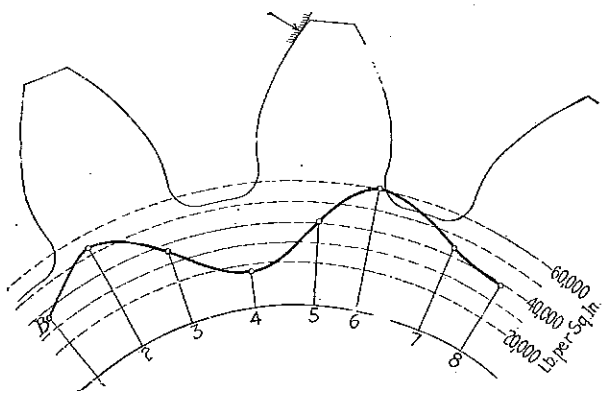

Fig. 19. Stresses along the Inside of Bore with Decreased Pressure (18,100 lb.) and Maximum Torque

60. When the inside radial pressure is increased in such proportion that without any torque being applied it produces stresses at the outside boundary of the gears of a magnitude approaching that due to the torque load, it will be this internal pressure which will have a preponderant influence.

61. Pinions have been examined with maximum values for $(\widehat{rr}-\theta\theta)$ of 60,000 and 81,500

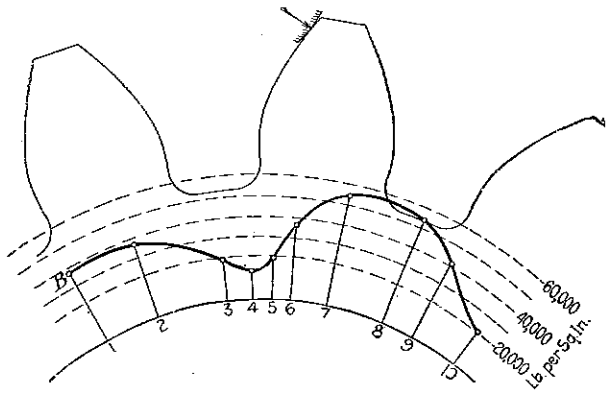

Fig. 18. Stresses along the Inside of Bore, with Normal Pressure (28,820 lb.) and Maximum Torque

TABLE VII

VALUES OF THE TANGENTIAL STRESS ALONG THE BOUNDARY OF THE LOADED TOOTH—TENSION SIDE

(Normal inside pressure—reduced torque)

No. of Point in Fig. 20	q Lb. per Sq. In.
1	39,700
2	51,500
3	58,500
4	57,700
5	56,600
6	51,500
7	38,000
8	19,500

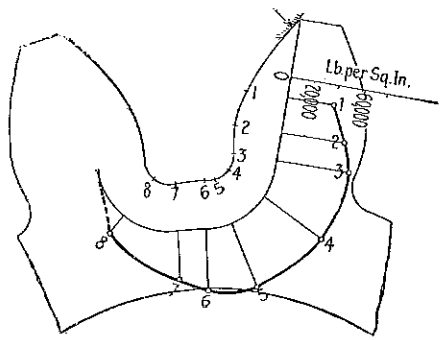

Fig. 20. Tangential Stress at Tension Side—Normal Inside Pressure and Reduced Torque

lb. per sq. in. at the inside boundary with the torque load at its normal value of 500 lb. tractive force per inch of face. The tractive force was afterward brought up to its maximum value of 1500 lb.

62. These tests showed that the torque load, when applied to the pinion subjected to those increased radial pressures, affects only the distribution of the stresses. It makes the high stresses extend over a larger area, but it does not increase materially the maximum stress. In these cases the dangerous section is no longer a straight section through the root of the tooth but it follows a V-shaped line, the lower point of which lies toward the inside bore. The sharpness of the angle of the V-shaped fracture at the base of the tooth appears to be due to an excess of radial shrinking pressure. In practice this excess is due to the pounding of the pinion onto the tapered shaft past its normal position.

63. In this connection a study was made of the stress distribution through two radial sections, passing respectively through the points A and B of the minimum cross-section of the main tooth, the points of maximum tension and compression.

64. The values of $(p-q)$ were deduced from the colored image of Fig. 4.* Extensometer measurements of $(p+q)$ were made. As before, the scales of both measurements were determined so that the stresses in the models shall represent the stresses in the steel pinion.

65. The maximum torque and the normal inside pressure were applied. Table VIII and Figs. 21 and 22 give the values obtained. Fig. 21 gives the magnitude of the principal stresses along the two sections AA' and BB'. Fig. 22 gives a portion of the lines of principal stress taken from Fig. 14, and for the same sections AA' and BB' shows the two principal stresses plotted in direction and in magnitude.

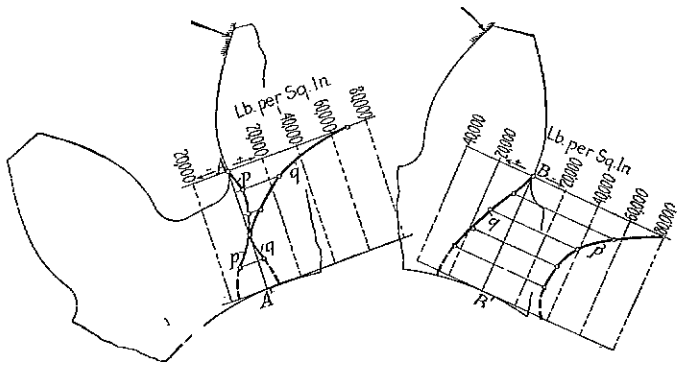

Fig. 21. Principal Stresses Across Radial Sections of Tooth—Normal Inside Pressure and Maximum Torque

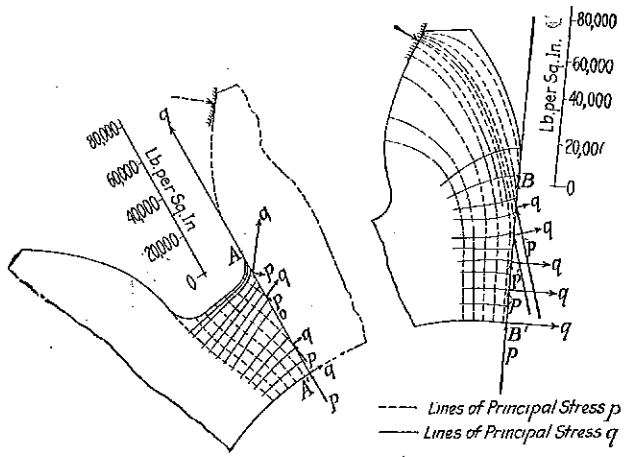

Fig. 22. Principal Stresses in Direction and Magnitude for Same Radial Sections as Those Shown in Fig. 21

*See Frontispiece of this issue of the REVIEW.

TABLE VIII

VALUES OF THE PRINCIPAL STRESSES ACROSS THE RADIAL SECTIONS PASSING RESPECTIVELY THROUGH THE POINTS *A* AND *B* OF THE MINIMUM CROSS-SECTION OF THE LOADED TOOTH

Cross-Section *BB'* Fig. 21; Distance in Inches from Point B'	p Lb. per Sq. In.	q Lb. per Sq. In.
0.410 (*B*)	−79,900	0
0.334	−55,800	6,000
0.256	−39,000	15,200
0.179	−32,600	18,400
0.102	−27,100	23,500
Cross-Section *AA'* Fig. 21; Distance in Inches from Point A'		
0.410 (*A*)	0	69,350
0.334	4,350	25,400
0.256	2,700	10,300
0.179	0	0
0.102	−11,350	3,350

66. A good way to visualize the state of stress at a given point is to consider a rectangular element with its sides parallel to the two principal stress directions at that point. By considering such elements along the sections *AA'* and *BB'* (Fig. 22) from this viewpoint, one can form a mental picture of how the section is acted upon by the elastic forces.

67. It would require too much space to include in this article a full discussion and to make a complete report of the results summarized here. The authors trust that the material they have presented will stimulate those interested in this subject to further efforts in the development and use of the photo-elastic method.

68. It seems, finally, almost superfluous to call attention to the comparative ease with which such a stress problem as this can be handled by the photo-elastic method, whereas the use of ordinary engineering methods gives untrustworthy results and the exact mathematical solution based upon the theory of elasticity is impossible.

69. Acknowledgment is due to the Massachusetts Institute of Technology for permission to use in this article certain of the results included in the thesis submitted by Dr. Paul Heymans, University of Ghent, Belgium, as partial fulfillment of the requirements for the degree of Doctor of Science from the Institute.